JOURNAL OF CATALYSIS 148, 709–721 (1994)

A Study of Anomalous Temperature-Programmed Reduction Profiles of Cu_2O, CuO, and CuO–ZnO Catalysts

G. Fierro,*,[1] M. Lo Jacono,* M. Inversi,* P. Porta,* R. Lavecchia,† and F. Cioci†

*Centro di Studio CNR "SACSO," c/o Dipartimento di Chimica, Università di Roma "La Sapienza," Piazzale Aldo Moro 5, 00185 Roma, Italy; and †Dipartimento di Ingegneria Chimica, Università di Roma "La Sapienza," Via Eudossiana 18, 00184 Roma, Italy

Received July 26, 1993; revised January 17, 1994

A temperature-programmed reduction (TPR) study of CuO, Cu_2O, and CuO–ZnO catalysts, in the atomic range Cu:Zn = 92:8 to 67:33, is reported. In order to promote a correct experimental approach, much attention has been devoted to the choice of the experimental operating variables. Direct evidence is presented that the reduction profiles of the investigated specimens are markedly affected by artefacts when TPR measurements are carried out under conditions of an inadequate combination of initial amount of reducible species, total flow rate, initial hydrogen concentration, and heating rate. It is shown that under correct experimental conditions the reduction profile of each sample is characterized by a single and quite sharp reduction peak. In contrast to this, a dramatic change of shape occurs when an improper combination of the experimental operating variables is imposed: for both CuO and Cu_2O an apparent double peak appears, whereas for the CuO–ZnO catalysts the reduction profiles are transformed into broad bands. In all cases, the reliability of the TPR results is completely lost.

To explain the complex origin of these artefacts, it is suggested that both a special dynamic situation and activated H_2 adsorption–desorption phenomena coinciding with the chemical reduction are responsible for the observed perturbations. A simple kinetic analysis has been developed which enables a qualitative reproduction of the disturbed reduction profiles to be made.

I. INTRODUCTION

Since its introduction by Robertson *et al.* (1), temperature-programmed reduction (TPR) has gained increasing application in the study of catalysts. It is no longer merely an ancillary technique: it has become a principal method to clarify important phenomena such as metal–support interaction (2, 3), the influence of pretreatment procedures on the reducibility of catalyst surfaces (4, 5), the role of metal additives as promoters of reduction (6, 7, 8), and, in multicomponent systems, the influence of one or more phases on the reducibility of a specific component (7). As emphasised by the numerous examples cited in the excellent monograph of Jones and McNicol (9), TPR has contributed greatly to the characterization of two classes of important industrial catalyst, namely (a) supported metals, especially bimetallics, and (b) transition-metal-exchanged zeolites.

However, in spite of the increasing use made of TPR, very few papers dealing with the theoretical basis of profile analysis have been published. In order to exploit the method to the highest degree and also to assess the reliability of results, we believe that it is necessary to obtain more insight into the dynamic and parametric sensitivity of the TPR technique. An important advance in this direction was effected in an excellent paper by Monti and Baiker (10), who analyzed the influence exerted on the reduction profiles by the experimental operating variables used in TPR. Typical TPR characteristics, namely the temperature which corresponds to the maximum of the reduction profile and the shape of the profile itself, are affected both by factors extrinsic to the technique, such as mass transfer limitations, and by the experimental operating variables. If the extrinsic effects are eliminated, a characteristic number $K = S_0/V^*C_0$, where S_0 is the initial amount of reducible species in the sample (μmol), V^* is the total flow rate (ml/s), and C_0 is the initial hydrogen concentration in the feed (μmol/ml), was defined by these authors to aid in selecting the values for the operating variables.

In order to obtain optimum reduction profiles K values have to range from 55 to 140 s for heating rates (β) of 6 K min^{-1} up to 18 K min^{-1}. Monti and Baiker conclude that for values of K below 55 s the sensitivity becomes too low, while for values of K exceeding 140 s the quantity of hydrogen consumed is too large, resulting in a violation of the assumption of a linear concentration profile.

More recently Malet and Caballero (11) published an important paper about the selection of experimental conditions in TPR experiments. Taking into account the Monti and Baiker criterion, they proposed a new parameter P, defined as $\beta S_0/V^*C_0$, in order to obtain unperturbed

[1] To whom correspondence should be addressed.

0021-9517/94 $6.00

reduction profiles. With respect to the Monti and Baiker characteristic number K(10), the use of the parameter P is more immediate as TPR runs may be carried out at different β, so avoiding every time the need of calculating the boundary conditions which vary on changing β (10). A comparison of theoretical TPR curves calculated at different values of P showed that above $P = 60$ the curves were markedly distorted and became flat at their maxima. These authors suggest that distortion or broadening of the TPR peak shape observed at high values of P is related to a situation in which the hydrogen content of the carrier is largely consumed; in fact, the perturbations become more evident as the hydrogen consumption in the feed is more close to completeness (11).

Taking into account the Malet and Caballero results and applying the Monti and Baiker approach, we have investigated the temperature-programmed reduction of CuO, Cu_2O, and some CuO–ZnO catalysts employing both adequate and inadequate experimental conditions. Preliminary results have been presented at the 10th International Congress on Catalysis (12). The present paper, on the other hand, reports in detail the overall study which we have accomplished on this subject, including additional results. Direct experimental evidence is provided that artefacts markedly perturb the TPR profiles of CuO, Cu_2O, and CuO–ZnO catalysts at high K values where the reliability of results is completely lost. Furthermore, with respect to CuO, it is shown that at low K values, even when belonging to the correct range, artefacts can also occur. Finally, an attempt is made to interpret qualitatively the shape of some perturbed TPR profiles on the grounds of hydrogen adsorption–desorption phenomena.

II. EXPERIMENTAL

A. Sample Preparation and Characterization

(i) CuO–ZnO catalysts. The CuO–ZnO catalysts had nominal atomic ratios Cu : Zn equal to 67 : 33, 77 : 23, 85 : 15, and 92 : 8. The preparation and characterization of both the precursors and calcined oxides have been reported in detail in other papers from our group (13, 14). Briefly, samples were prepared starting from hydroxycarbonates as precursors which were obtained at constant pH 8 by adding suitable copper and zinc nitrate solutions to a $NaHCO_3$ solution at 333–343 K under vigorous stirring; these precursors are monophasic or biphasic depending on their relative composition (13). However, each phase homogeneously assembles copper and zinc in the same lattice and a good interdispersion of the two phases [zincian malachite, $Zn_xCu_{2-x}(OH)_2CO_3$ and aurichalcite, $(Zn,Cu)_5(CO_3)_2(OH)_6$] is obtained (13, 14). As a consequence, when the precursors are thermally decomposed at 623 K in air, the nucleation and growth of the CuO–ZnO particles can occur almost simultaneously producing well dispersed fairly uniform mixed oxides with CuO and ZnO crystallite sizes always below 100 Å (15).

The experimental copper and zinc content was determined by atomic absorption spectroscopy of the hydroxycarbonate precursors and for each sample it was very close to the nominal values (13, 14).

Total surface areas (S.A.) were measured by the BET method, using nitrogen ($\sigma_{N_2} = 0.162$ nm^2) or krypton ($\sigma_{Kr} = 0.195$ nm^2) as the adsorbate.

The crystallite sizes (D) of CuO and of ZnO were determined by X-ray line broadening from the half-width of the (111)-(200) ($2\theta = 38.8°$) and (100) ($2\theta = 31.8°$) reflections for CuO and ZnO, respectively, after correction for instrumental broadening, using the Scherrer equation, $D = K\lambda/\beta \cos\theta$ with $K = 1$ (15, 16).

Some results dealing with the characterization of the calcined oxides are summarized in Table 1.

(ii) Copper(II) oxide. Cupric oxide was prepared according to the following methods: (a) by precipitation at constant pH 8, as for the CuO–ZnO catalysts, and (b) at variable pH (rising from 4 to 8). The latter method, already reported by Herman *et al.* (17), is based on the dropwise addition at 333 K of a sodium carbonate solution to a well stirred copper nitrate solution. Different monophasic precursors were obtained from the two methods: copper hydroxycarbonate [malachite, $Cu_2CO_3(OH)_2$, ASTM 10-399] and copper hydroxynitrate [gerhardtite, $Cu_2(NO_3)_2(OH)_2$, ASTM 14-697, 15-14] in the first and second preparation, respectively (13, 17). Precursors were then dried overnight at 393 K and finally calcined at 623 K for 24 h. In Table 1 the results of the characterization of calcined samples are reported.

(iii) Copper(I) oxide. Cuprous oxide was prepared by heating the cupric oxide obtained from decomposition of the malachite-like precursor in a furnace at 1373 K for 19 h. The XRD pattern was typical of Cu_2O and, within the sensitivity of the technique, no reflections belonging to CuO were detected.

B. Temperature-Programmed Reduction

(i) Apparatus. The TPR apparatus, designed and constructed in our laboratory, consists of two parts: (1) a flow system to perform the TPR measurements by applying a stream of diluted hydrogen, and (2) a vacuum line where sample pretreatment, trapping of the water released during the reduction, and measurement of its quantity can be effected (19). The flow circuit was connected to the vacuum line as shown schematically in Fig. 1.

In more detail the continuous-flow section of the apparatus consists of: (i) a zone where ultrapure H_2 (99.999%), N_2 (99.999%), O_2 (99.995%), and He (99.995%) are stored in bottles; (ii) a 4-channel electronic mass-flow controller (UCAR Instruments, Model MFB 30) for fixing accurately

TABLE 1

TPR and Characterization Results for CuO, Cu_2O, and CuO–ZnO[a]

Sample Cu : Zn	TPR run	T_M (K)	$P = K \cdot \beta$ (K)	$K = S_0/V^*C_0$ (s)	$W_{1/2}$ (K)	Loading (g)	S_0 (μmol)	S.A. (m^2/g)	D(Å) CuO–ZnO	
100 : 0	27	50A	12	148	30	0.02040	250	40	140	—
100 : 0	8A	518	97	1166	106	0.07710	970	40	140	—
		562								
100 : 0	50	468	5.4	65	39	0.00910	110	40	140	—
		558			52					
100 : 0[b]	34	519	12.3	148	33	0.02010	250	40	140	—
92 : 8	36	477	11.2	134	29	0.01960	226			
	54A	555	116	1393	115	0.10180	1176	71	90	90
		573								
85 : 15	28	483	10.8	130	21	0.02070	220	71	90	90
	10A	555	109.8	1318	94	0.10290	1096			
		576								
77 : 23	29	475	11	132	24	0.02300	223	74	65	100
	13A	550	128	1542	102	0.13190	1282			
		575								
67 : 33	30	480	10.8	130	22	0.2640	220	74	65	100
	18A	573	105	1263	103	0.12570	1050			
CuO[c]	35	517	11.3	136	54	0.01790	230	2.4	>800	—
Cu_2O	38	528	9.8	118	38	0.02880	200			
	16A	552	104	1250	118	0.14960	1040			
		591								

Note. Experimental conditions: $\beta = 5$ K min^{-1}; stream, 6% (v) H_2 in N_2; V^* = (i) 40 ml (STP) min^{-1} and (ii) 20 ml (STP) min^{-1} for runs labelled "A."

[a] For explanation of symbols, see text.

[b] Sample prepared by pressing the powder into pellets which have been ground and sieved within 425–850 μm range.

[c] Sample obtained by decomposition of copper hydroxide nitrate (gerhardtite) as precursor.

the flow rates of each gas; (iii) a set of blending boxes for the preparation of various gas mixtures; (iv) a set of three-way valves which directs the stream towards different pathways of the gas-flow system and connects the reactor to the vacuum line.

Nitrogen-diluted hydrogen crossed, at a fixed rate, the reference compartment, a hot wire (HW) detector from Carlo Erba (Model HWD 450), then the reactor containing the catalyst, and, finally, via a cold trap, the other compartment of the HW detector. The HW detector sensitivity was determined for all experimental conditions employed in this work and the linearity of the output signal obtained with respect to the hydrogen concentration was checked and always verified.

A temperature controller (Leeds & Northrup Instruments, Model Electromax V Plus) was used both for increasing the furnace temperature with linear heating rates and for keeping it constant at any selected value.

Both the rate of hydrogen consumption and the heating rate β were monitored on a multichannel chart recorder (Leeds & Northrup Instruments, Model Speedomax 2500).

A quartz-glass reactor with a porous septum (ca. 10 mm in diameter), over which the specimens were spread out, was used. The quartz-glass reactor together with the furnace resembled those adopted by Cvetanović and Amenomiya (20).

The volume of the tubing between the reactor and detector was minimized in order to eliminate dispersion effects which can perturb the shape of the TPR profiles (10). For this purpose capillaries of stainless steel were used to connect the reactor to the reference and measurement compartments of the hot wire detector.

(ii) Experimental procedure. Samples used in the TPR measurements have the consistency of a fine powder and particle sizes (measured by sieving) less than 100 μm. The reactor was loaded with a suitable quantity of specimen in order to have different amounts of copper to be reduced. The desired values of the characteristic number K were calculated according to the empirical equation introduced by Monti and Baiker (10).

Before starting a TPR run, each sample was pretreated *in situ* under flowing oxygen at 573 K for 1 h, followed by a nitrogen flow for 0.33 h. In the case of Cu_2O samples only pure nitrogen flow was used. The sample was then cooled in nitrogen to room temperature and was maintained at room temperature for 0.5 h. Next the reducing blend was formed by mixing the nitrogen and hydrogen flows in a suitable proportion, the trap was cooled with

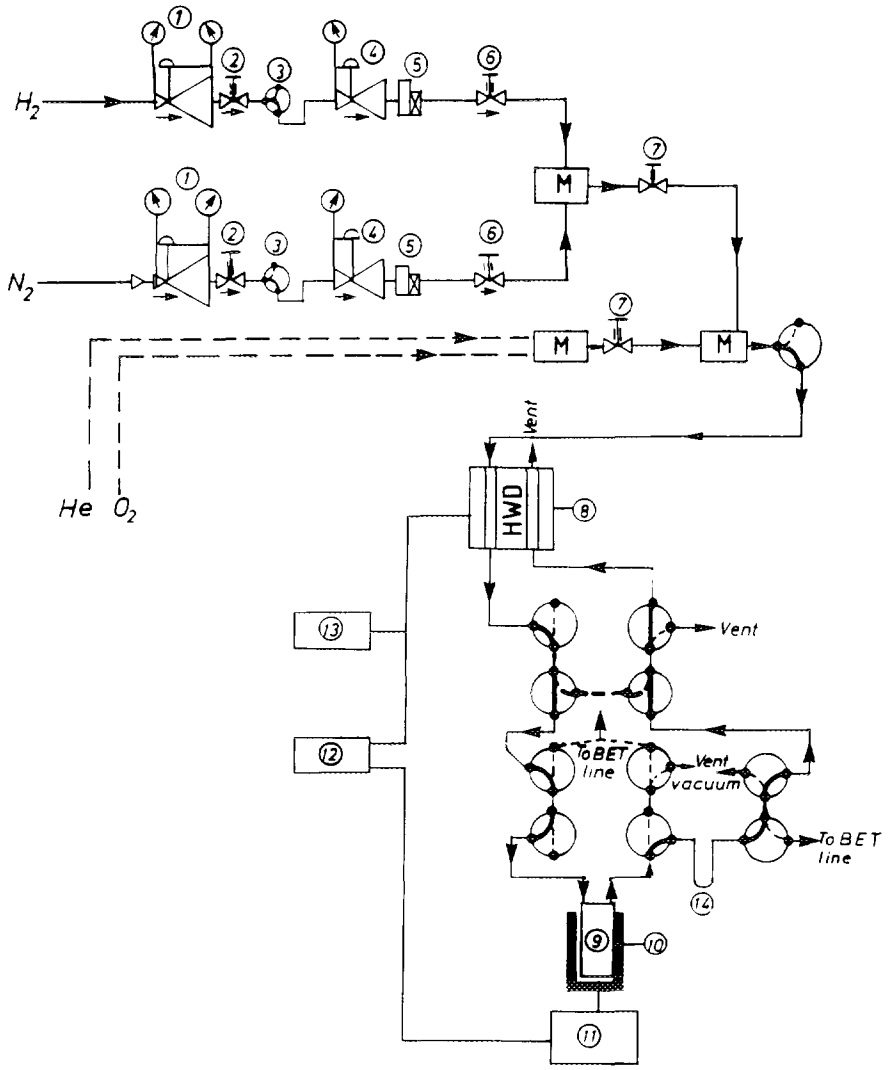

FIG. 1. Schematic diagram of the TPR apparatus. (M) Blending box, (1) two-stage pressure regulating valve, (2) needle valve, (3) three-way valve, (4) back pressure valve, (5) electronic mass flow controller, (6, 7) inflow valves, (8) hot wire detector, (9) reactor, (10) furnace, (11) temperature controller, (12) recorder, (13) hydrogen consumption integrator, and (14) cooling trap (78 K) filled with glass spheres. The dotted lines indicate that two other apparatus sections, analogous to those represented in detail from (1) to (6) for hydrogen and nitrogen, exist for helium and oxygen, respectively.

liquid nitrogen, and the stabilization of the baseline of the HW detector was monitored. V^* will be used to signify the volumetric flow rate.

A standard TPR run consisted of (i) an initial treatment in the gas flow at room temperature for 0.01 h, (ii) temperature programming, (iii) keeping the sample at the final temperature for 0.33 h, and (iv) outgassing of the sample at the final temperature for 0.33 h. The heating rate was fixed at 5 K min^{-1}, unless otherwise stated.

The total hydrogen consumption was determined in two ways: (a) by transmitting the HW detector output to an amplification and integration system (Shimadzu Instruments, Model Chromatopac CR1B); (b) by estimating the water released during the reduction through a stepwise expansion into a calibrated zone of the vacuum line.

TPR profile peaks were usually characterized by the temperature corresponding to the maximum hydrogen consumption rate, T_M, and the full width at half maximum, $W_{1/2}$ (see Table 1).

III. RESULTS

A. Mass Transfer Limitations and Dispersion Effects

As mass transfer effects have a detrimental influence on the shape of TPR profiles, it is necessary to verify that the TPR measurements are not affected by both inter- and intra-particle mass transfer limitations.

The influence of internal diffusion is generally determined by calculating a dimensionless number, the Thiele modulus, ϕ, which is a measure of the ratio between the

surface reaction rate and the rate of diffusion through the solid particle. When the Thiele modulus is large, diffusion is likely to affect the overall reaction rate, whereas when it is small the surface reaction is usually rate determining. Ibok and Ollis (21) applied this criterion for checking pore diffusion limitations in TPD experiments but the same analysis can be made for TPR experiments. The above authors found that for ϕ values less than 0.3 no appreciable diffusion gradients exist within the pellet. A ϕ value equal to 0.3 corresponds to a critical particle radius of 400 μm, so that experiments carried out with particles having radii of 400 μm or less are not expected to be influenced by intra-particle mass transfer limitations.

The occurrence of inter-particle limitations is evaluated on the basis of the Sherwood number, which represents the ratio between the mass transfer and diffusion rates. Also for this parameter a limiting value exists above which the external mass transfer does not affect the overall reaction rate.

Although we did not determine the Thiele modulus and the Sherwood number, our TPR measurements were made employing samples with particle sizes less than 100 μm, under conditions similar to those used by Monti and Baiker (10), who verified the absence of mass transfer limitations. Therefore we can infer that the results obtained by us are also not affected by internal or external mass transfer limitations.

However, the two criteria for diffusional retardation should be used just for a preliminary rough estimate. It is more advisable to perform experiments which, having chosen the experimental conditions, provide direct evidence for the absence or presence of mass transfer limitations. In line with this, we have carried out some TPR experiments with pure CuO, obtained from malachite as a precursor, employing two fractions with different particle sizes. The first fraction (run 27) was the powder as prepared, having particle sizes less than 100 μm; the second one (run 34) was obtained by pressing the powder into pellets which were further gently ground in a mortar and sieved in the range 425–850 μm. In Fig. 2A the reduction profiles obtained at K = 148 s are reported. Note that the CuO pellets sieved in the range 425–850 μm have a lot of particles which may cause diffusional retardation. A shift (15 K) of T_M toward higher values is observed (see Table 1, lines 1 and 4) and a slight shoulder appears on the low temperature side; however, the peak shape does not change significantly.

Moreover, Fig. 2B reports the reduction profiles of two CuO samples prepared from different precursors and distinguished by a large difference of surface area to which, in turn, the ratio of surface/bulk oxide ions is related. TPR profiles of both samples are characterized by a single reduction peak; on decreasing the surface area, the T_M value shifts slightly towards higher temperature and the peak width increases, but no other peaks appear. In conclusion, even though the results in Fig. 2 are not direct evidence for the absence of mass transfer limitations, they show clearly that inter- and intra-particle mass transfer limitations, when present, do not lead to a double peak profile.

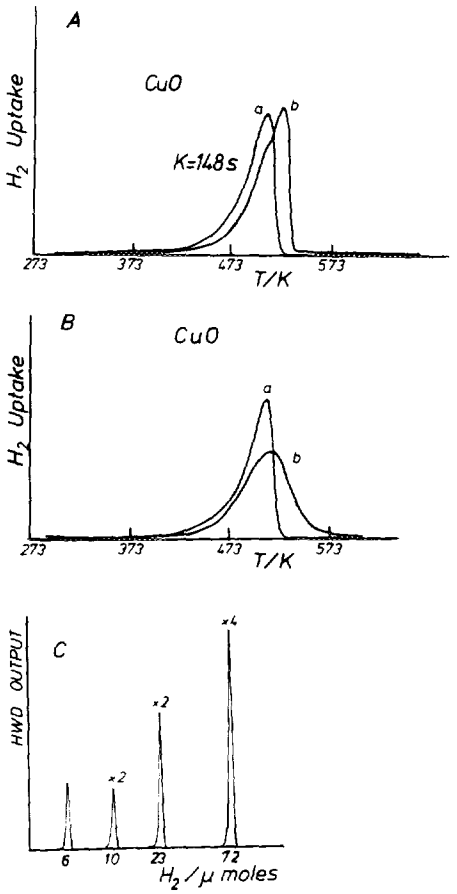

FIG. 2. Checking for mass transfer limitations and dispersion effects on TPR profiles. (A) TPR profiles of two CuO batches having different particle sizes: (a) less than 100 μm (run 27); (b) between 425 and 850 μm (run 34). (B) TPR profiles of CuO samples having different surface areas: (a) CuO obtained from malachite, S.A. = 40 m^2g^{-1} (run 27); (b) CuO obtained from gerhardtite, S.A. = 2.4 m^2g^{-1} (run 35). (C) Output of the hot wire detector (HWD) as a function of the amount of hydrogen (see text). Carrier gas, N_2; flow rate, 20 ml (STP) min^{-1}.

In addition to diffusion effects, dispersion of the original signal caused by the volume of the tubing (10) was checked in our apparatus. Experiments were carried out in which small quantities of pure hydrogen were withdrawn from the calibrated zone of the vacuum section and then directly driven away by nitrogen flowing at 20 ml (STP) min^{-1} through the unloaded reactor and HW detector. In Fig. 2C the HW detector outputs, obtained for different amounts of hydrogen, are reported. No baseline drifts are

present and each peak is characterized by a Gaussian-type shape.

In Figs. 3 and 4 the TPR profiles, obtained either at adequate or at inadequate values of the characteristic number K, are reported for Cu_2O, CuO, and CuO–ZnO catalysts, respectively.

B. Temperature-Programmed Reduction of Copper(I), Copper(II) Oxides, and CuO–ZnO Based Catalysts

In Figs. 3 and 4 the TPR profiles, obtained for either adequate or inadequate values of the characteristic number K, are reported for Cu_2O, CuO, and CuO–ZnO catalysts, respectively. Table 1 lists results derived from the TPR measurements and the principal experimental parameters.

Either the integrated hydrogen consumption or the amount of trapped water indicated that each sample was completely reduced to metallic copper at the TPR run conditions.

TPR profiles of both Cu_2O and CuO obtained at inadequate high value of K [Figs. 3A and 3B]; TPR runs 16A and 8A in Table 1, respectively] are characterized by a wide and unexpected double peak which is less pronounced for Cu_2O than for CuO (see Fig. 3).

Contrary to this, the shape of the reduction profiles obtained at adequate values of K (TPR runs 38 and 27 in Table 1, respectively) are completely different from those characterized by inadequate high K values: in fact, by using K values equal to 118 and 148 s, the TPR profiles of Cu_2O and CuO appear as single and quite sharp peaks (Figs. 3A and 3B).

The reduction profile of CuO with a low K value of 65 s (obtained by a low sample loading, TPR run 50 in Table 1) also showed a double peak (see Fig. 3B) even though this value of K belongs to the adequate range; at first this result was confusing, but when the TPR run was completed and the furnace was removed we observed the formation of a mirror of metallic copper on the reactor walls. This was an indication that an anomalous reduction process had occurred. In order to clarify this aspect two TPR measurements were carried out in which the CuO load was increased together with the H_2 concentration and the feed rate [10% (v) H_2 in N_2, V^* = 90 ml (STP) min^{-1}], in one case for preserving the K value of 65 s and, in the second case, for obtaining a lower value of K. The corresponding results are illustrated in Fig. 3C: in both cases a single and quite sharp reduction peak was observed. For the sake of comparison, the TPR profile with K = 65 s (TPR run 50 in Table 1), characterized by a double peak, is also reported in Fig. 3C.

CuO was further submitted to a set of TPR experiments in which inadequate high values of K (ca. 1100 s) were

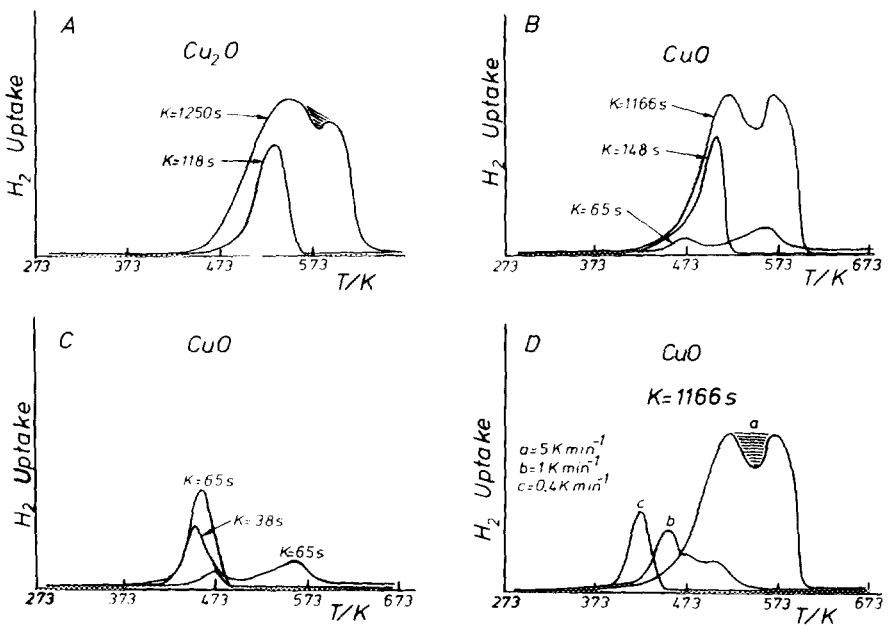

FIG. 3. Temperature-programmed reduction of Cu(I) and Cu(II) oxides. (A) Cu_2O: run 38, K = 118 s; run 16A, K = 1250 s. This is a repeated experiment from Ref. (12). (B) CuO from malachite: run 27, K = 148 s; run 8A, K = 1166 s; run 50, K = 65 s. This is a repeated experiment from Ref. (12). (C) CuO from malachite. Conditions: β = 5 K min^{-1}; 10% (v) H_2 in N_2; V^* = 90 ml (STP) min^{-1}; sample loadings: for K = 65 s and $P = (K \cdot \beta)$ = 5.4 K, 0.03490 g; for K = 38 s and P = 3.17 K, 0.02030 g. For the sake of comparison the reduction profile of run 50 (sample loading: 0.00910 g, K = 65 s) is also reported. (D) CuO from malachite at fixed high K value (ca.1100 s) and different heating rate. Conditions for (b) and (c): 3% (v) H_2 in N_2, V^* = 40 ml (STP) min^{-1}, sample loadings = 0.07600 g, P(b) = 18.3, P(c) = 7.3. The reduction profile (a) of run 8A is also reported; P(a) = 97.

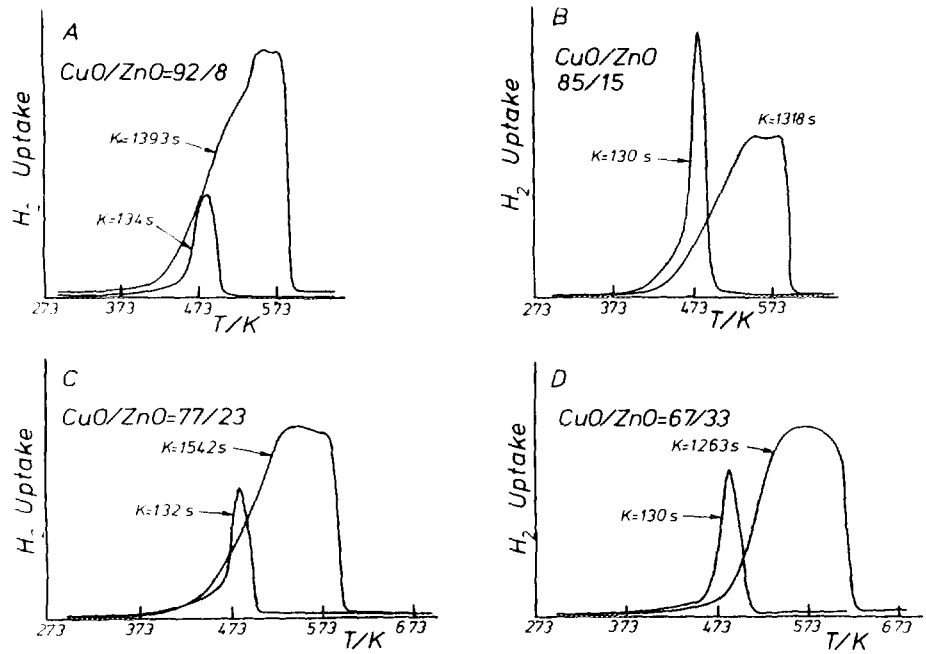

FIG. 4. TPR of CuO–ZnO catalysts as measured under adequate (K = 118 s) and inadequate (high K value) experimental conditions: (A) CuO : ZnO = 92 : 8 (runs 36 and 54A). (B) CuO : ZnO = 85 : 15 (runs 28 and 10A). (C) CuO : ZnO = 77 : 23 (runs 29 and 13A). (D) CuO : ZnO = 67 : 33 (runs 30 and 18A). In (C, D) repeated experiments from Ref. (12) are reported.

fixed and the heating rate, β, was decreased from 5 to 0.4 K min^{-1} in order to obtain different values of P (11) in the range 100–10 K; the reduction profiles so far obtained are reported in Fig. 3D.

With regard to the CuO–ZnO mixed oxide catalysts, their reduction profiles (Fig. 4) also showed a dramatic change of shape on going from inadequate (TPR runs 54A, 10A, 13A, and 18A in Table 1) to adequate (i.e., correct) K values (TPR runs 36, 28, 29, and 30 in Table 1). At correct K values, single and sharp peaks characterize the TPR profiles which are transformed, as expected, into broad bands when high K and P values are imposed. In each of the TPR experiments both the measured hydrogen consumption and the amount of trapped water were in agreement with a complete reduction to metal copper. The maxima of the sharp reduction peaks obtained under correct experimental conditions are located at about 480 K, a value 24 K lower than that found for pure CuO under similar experimental conditions. On the other hand, the maxima of the broad bands obtained at inadequate K values, being spread out are therefore not well defined. However, except for the Cu : Zn = 67 : 33 sample, we have tried to trace two maxima whose T_M values are reported in Table 1.

C. Kinetic Model and Simulation of the TPR Artefacts

A theoretical analysis of TPR profiles can be performed by solving the rate equation for the reduction process under non-isothermal conditions (10)

$$dn/dT = 1/\beta\,(dn/dt) \qquad [1]$$

together with the mass balance equation for hydrogen

$$V^*C_0 - V^*C_e + dn/dt = 0 \qquad [2]$$

where dn/dt is the hydrogen consumption rate, β is the heating rate equal to dT/dt, C_0 and C_e are the inlet and outlet hydrogen concentrations, respectively, and V^* is the volumetric flow rate. If the process is not influenced by external or internal mass transfer limitations, the hydrogen consumption rate is determined only by the chemical reaction rate. In particular, for the reaction

$$MeO + H_2 \rightarrow Me + H_2O$$

the general expression

$$dn/dt = -kS_{MeO}C_{H_2} \qquad [3]$$

can be used, where S_{MeO} is the amount of the reducible species, C_{H_2} is the concentration of the hydrogen, and k is a temperature-dependent rate constant for which the Arrhenius relationship can be assumed:

$$k = k_0 \exp(-E_A/RT). \qquad [4]$$

If in a TPR experiment a small amount of catalyst is used and the conversion of the reactants is low, the hydrogen concentration throughout the reactor can be assumed uniform and equal to the arithmetic mean between the inlet and outlet concentrations:

$$C_{H_2} = (C_0 + C_e)/2. \quad [5]$$

Note that the reactor can be considered gradientless, with a spatially uniform reaction rate only at low conversion. After substitution of Eq. [4] into Eq. [3], and of Eqs. [2] and [5] into Eq. [1], one obtains:

$$dn/dT = (-2C_0V^*/\beta)[S_{MeO}k_0 \exp(-E_A/RT)]/[2V^* + S_{MeO}k_0 \exp(-E_A/RT)]. \quad [6]$$

A numerical integration of Eq. [6] with the initial condition

$$S_{MeO} = S_{0_{MeO}} \text{ at } t = 0 \quad [7]$$

leads to a simulated TPR profile.

The hydrogen uptake as a function of temperature gives rise to a single asymmetric peak whose shape and position are determined by the values of the operating variables (heating rate, hydrogen flow rate, and concentration) and of the kinetic parameters (pre-exponential factor and activation energy). In order to provide evidence for this theoretical consideration, simulated TPR profiles were generated by integrating Eq. [6] under different operating conditions. The influence of the variables C_0, V^*, and β was investigated at constant S_0 and for fixed values of the kinetic parameters, k_0 and E_A, according to the scheme reported in Table 2. The results are shown in Fig. 5. It clearly appears that all simulated TPR profiles exhibit only one peak, regardless of whether the operating conditions meet or do not meet the criteria proposed by Monti and Baiker for reliable experimental profiles, i.e., $0.33 < C_M/C_0 < 0.9$ (10).

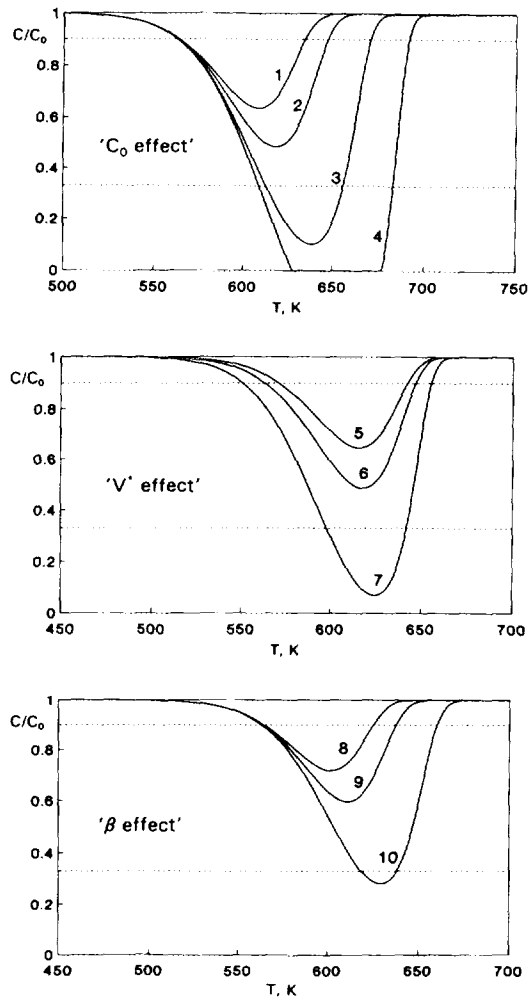

FIG. 5. Simulated TPR profiles under different operating conditions as reported in Table 2. Fixed parameters: S_0 = 300 μmol, $k_0 = 3 \times 10^{10}$ cm³/mol s, E_A = 150 kJ/mol.

TABLE 2

Parameters Adopted for Simulated TPR Profiles (S_0 = 300 μmol, $k_0 = 3 \times 10^{10}$ cm³/mol s, E_A = 150 kJ/mol)

Profile	C_0 (μmol/cm³)	V^* (cm³/s)	β (K/s)	K (s)
1[a]	3.0	1.0	0.20	100
2[a]	2.0	1.0	0.20	150
3[b]	1.0	1.0	0.20	300
4[b]	0.6	1.0	0.20	500
5[a]	2.0	1.5	0.20	100
6[a]	2.0	1.0	0.20	150
7[b]	2.0	0.5	0.20	300
8[a]	2.0	1.0	0.10	150
9[a]	2.0	1.0	0.15	150
10[b]	2.0	1.0	0.30	150

[a] Operating conditions within the boundary conditions reported by Monti and Baiker (10).

[b] Operating conditions outside the boundary conditions reported by Monti and Baiker (10).

It seems noteworthy to stress that the limits on the characteristic number K (55 s $< K <$ 140 s) do not provide an absolute criterion, since they change either with the heating rate (β) or with the chemical nature of the investigated system (k_0, E_A). In fact the lower limit (55 s) is relative to a heating rate of 6 K min^{-1} and the upper one (140 s) to 18 K min^{-1}. Furthermore, both limits have been determined by using the kinetic parameters (k_0 and E_A) of nickel oxide and hence they should be used, strictly speaking, only for the reduction of this species. A more appropriate procedure would consist in deriving the two K limits from the validity range of C_M/C_0 ratio (i.e., 0.33

$< C_M/C_0 <0.9$) after calculating the TPR profiles with the actual values of k_0, E_A (to be estimated from the experimental data), and β. The effects of β and E_A on the minimum hydrogen flow rate at the reactor outlet are shown in Fig. 6, where the dashed lines delimit the region of adequate operating conditions. As can be seen, the lower limit of K is not too sensitive to β and E_A, whereas the upper one varies significantly. Obviously, situations may occur in which, for a given amount of the reducible species and for low hydrogen feed rates, the hydrogen present in the reactor is entirely consumed by reduction, giving rise to a flattened peak such as that represented by the TPR profile 4 of Fig. 5. These results point out that the artefacts observed by us and especially the double peak in the reduction profiles of CuO and Cu_2O cannot be interpreted by this simple kinetic model.

Although the present work is not aimed at a rigorous kinetic analysis of the reduction phenomena, we wish to stress that an adsorption–desorption step for hydrogen in parallel with chemical reaction can justify qualitatively the observed artefacts. For such a physical situation the kinetic scheme

$$MeO + H_2 \rightarrow Me + H_2O$$

$$H_2 + 2\sigma \leftrightarrow 2H^*$$

should be considered, where σ is a generic adsorption site on the solid and H* represents dissociatively chemisorbed hydrogen. It is important to point out that the term "adsorption–desorption" introduced here has a wider meaning and implies not only surface processes but also bulk processes, such as hydrogen trapping inside the crystal lattice. These phenomena which occur both in oxides and metals will be discussed in the next section.

The net rate of hydrogen adsorption can be expressed by a Langmuir-type equation as

$$dn_a/dt = -k_a C_{H_2}(1 - z)^2 + k_d z^2, \quad [8]$$

where z is the fraction of occupied sites, and k_a and k_d are the temperature-dependent rate constants for adsorption and desorption, respectively. Taking into account Eq. [8], the overall rate of hydrogen "consumption" can be rewritten as follows:

$$dn'/dt = -kS_{MeO}C_{H_2} - k_a C_{H_2}(1 - z)^2 + k_d z^2. \quad [9]$$

With respect to Eq. [3], the peculiarity of Eq. [9] is based on the fact that it contains terms by which not only disappearance but also appearance of hydrogen is introduced. The rate of hydrogen disappearance results from the contributions of the reduction and the adsorption processes, whereas the desorption term defines the rate of hydrogen appearance. Furthermore, Eq. [9] indicates that for the reduction of a given sample, at a fixed hydrogen flow rate and concentration, the weight of each term in the overall rate is dependent primarily on the values of the rate constants k, k_a, and k_d. Substituting Eq. [9] in Eq. [2] and rearranging, we obtain:

$$V^*C_e = V^*C_0 - [kS_{MeO}C_{H_2} + k_a C_{H_2}(1 - z)^2] + k_d z^2. \quad [10]$$

Qualitative observations about the onset of artefacts in the TPR profiles can be made if Eq. [10] is coupled to an analysis concerning the dynamics of a TPR experiment carried out under inadequate experimental conditions. At high K values the initial amount of the reducible species (S_0) is much higher than the feed rate (V^*C_0) of the reductant. As a consequence, when the reaction rate reaches its maximum at the peak maximum of the TPR profile, the

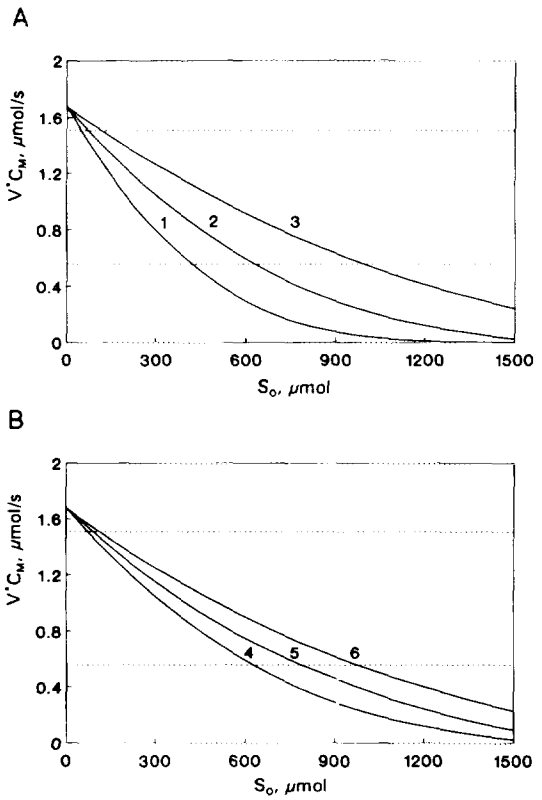

FIG. 6. Effect of β (A) and E_A (B) on the minimum hydrogen flow rate at the reactor outlet. (C_0 = 2.52 μmol cm^{-3}; V^* = 0.67 cm^3 s^{-1}; $k_0 = 1 \times 10^9$ cm^3 mol^{-1} s^{-1}).

(1) E_a = 80 kJ mol^{-1}, β = 0.133 K s^{-1}; [30 < K (s) < 255]
(2) E_a = 80 kJ mol^{-1}, β = 0.083 K s^{-1}; [55 < K (s) < 380]
(3) E_a = 80 kJ mol^{-1}, β = 0.050 K s^{-1}; [70 < K (s) < 595]
(4) E_a = 80 kJ mol^{-1}, β = 0.083 K s^{-1}; [55 < K (s) < 380]
(5) E_a = 100 kJ mol^{-1}, β = 0.083 K s^{-1}; [60 < K (s) < 415]
(6) E_a = 130 kJ mol^{-1}, β = 0.083 K s^{-1}; [65 < K (s) < 570]

rate of hydrogen disappearance, that is the term $[kS_{MeO}C_{H_2} + k_aC_{H_2}(1 - z)^2]$ in Eq. [10], is very large and can be similar to the H_2 feed rate. In this condition the hydrogen content of the carrier can be almost completely consumed, namely:

$$V^*C_0 - [kS_{MeO}C_{H_2} + k_aC_{H_2}(1 - z)^2]_{Max} \cong 0. \quad [11]$$

Under these conditions and setting equal to a constant the difference expressed in Eq. [11], Eq. [10] becomes:

$$V^*C_e \cong \text{const.} + k_dz^2. \quad [12]$$

Equations [11] and [12] will be satisfied as long as the amount of the unreduced sample is large enough to exhaust the hydrogen in the feed. Moreover, Eq. [12] implies that during this time the outlet hydrogen concentration may be equal to the amount of desorbed hydrogen, apart from a constant. Therefore, if no hydrogen desorbs, the output signal of the hydrogen detector remains constant and unchanged with respect to the value of the maximum reaction rate. It follows that the TPR peaks will become flat at their maxima and a broadening of the reduction profiles will occur. This analysis is indeed supported by the simulated TPR curves at high P values reported by Malet and Caballero for a single reduction process (11). On the other hand, when hydrogen desorption takes place this will be displayed as a hydrogen enrichment of the gas stream [see Eqs. [10] and [12]]. In this case the inverted signal polarity of the hydrogen detector may give rise to an inverted peak which, superimposed on the flat maximum of the reduction peak, produces an apparent double peak. The shaded areas in Figs. 3A and 3D would represent the supposed hydrogen desorption peaks.

Results concerning a simulation of the detector response, by assuming a Gaussian distribution for both the reduction and the desorption peak, are plotted in Fig. 7. We can observe that when small amounts of hydrogen desorb (less than 2%), only a broadening of the reduction profile is obtained. On the contrary, when hydrogen desorbs to a greater extent (4 and 6% in the simulation) two apparent and fairly well resolved peaks appear.

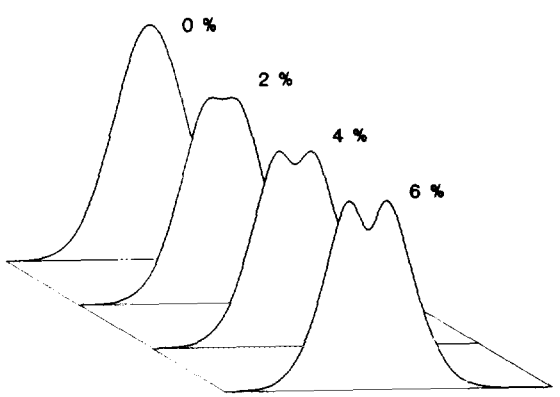

FIG. 7. Effect of percentage desorbed hydrogen amount on simulated TPR profiles.

IV. DISCUSSION

The most relevant feature arising from TPR profiles of Cu_2O, CuO, and CuO–ZnO mixed oxides is the dramatic change of their shape, i.e., the appearance of the double peak and/or the broadening of the profiles, when values of the quantity K much higher than 140 s are used.

The reduction profiles of CuO reported in previously cited papers (1, 6, 11) show a single reduction peak whose width at half maximum was not much larger than that found by us for the CuO specimens obtained by decomposition of two different precursors. However, the TPR profiles of CuO, CuO–ZnO, and CuO–ZnO/Al_2O_3 samples reported by Fleisch and Mieville (22) resemble the rather broad bands similar to those reported in this work when high values of K were used. It follows that the reduction profiles reported by Fleisch and Mieville for CuO and copper-based catalysts seem to suffer from some perturbations which, if they are not induced by an inadequate choice of the experimental operating variables, may be ascribed to mass transfer limitations or dispersion effects. A TPR study of the copper reducibility in CuO–ZnO catalysts will be reported in a forthcoming paper (23).

The onset of a double peak in the reduction profile of CuO when a low but adequate K value was used (see Figs. 3B and 3C) requires a special comment as in this case the reduction process was perturbed by sublimation of copper species. In fact, when the TPR run was completed (at the final temperature of about 673 K) a mirror of metallic copper was observed on the reactor walls. Since just a few milligrams of pure copper oxide was loaded in the reactor for obtaining a low K value (see TPR run 50 in Table 1), this amount was completely spread out over the porous septum, leaving the largest part of its area uncovered. Our hypothesis is that, at the beginning of the reduction, very small particles of metallic copper were formed because the sintering was hampered by a good dispersion and isolation of CuO particles physically dispersed over the porous septum. On increasing the temperature as the TPR run proceeds, these small particles of metallic copper could have enough energy to sublime thus covering the reactor walls and also the unreduced CuO particles. The reduction of the latter particles was probably hindered by the copper film, the hydrogen having to diffuse through it before reaction with the CuO particles.

Therefore, a second reduction peak appears at higher temperatures and the TPR profile takes a double-peak shape. Our hypothesis is indeed supported by another

TPR profile obtained at the same value of K equal to 65 s. The low K value was now attained by increasing both the CuO loading and the total flow rate (see Fig. 3C). This profile is characterized by a single reduction peak like that observed at a K value of 148 s (see Fig. 3B). Furthermore, on decreasing the K value to 38 s (which is a value outside the adequate range as indicated in Ref. (10)) the shape of the reduction profile remains unchanged showing again a single peak (see Fig. 3C). In both the latter TPR measurements, carried out by employing low K values of 65 and 38 s, the CuO loadings were high enough to avoid the sublimation of copper species so that Gaussian-type reduction peaks were formed.

On the other hand, at K values much higher than 140 s, which represents the most common case, the observed artefacts have a different nature. Monti and Baiker (10) pointed out that for K values exceeding 140 s (when β is in the range from 6 K min^{-1} to 18 K min^{-1}) the fraction of hydrogen consumed is too large, so that the assumption of a linear concentration profile inside the reactor is severely violated. Otherwise, the criterion that the amount of hydrogen consumed at the peak maximum had not to exceed $\frac{2}{3}$ of the hydrogen feed to the reactor is no longer fulfilled (10). This explanation agrees with the fact that the detector response at the peak maximum (1.27 mV), for runs 8A and 16A, is very close to the value corresponding to the total exhaustion of the hydrogen feed (1.33 mV). Accordingly, it would be expected (see section C of Results and Ref. (11)) that TPR measurements performed outside the boundary conditions resulted in a broadening and flattening of the reduction profiles; to our knowledge no experimental evidence of these phenomena has hitherto been shown in the literature. On the other hand, the onset of a double peak in the reduction profiles of both CuO and Cu_2O at high K values, which has never been reported and discussed, cannot be interpreted by the kinetic model regardless of whether the operating conditions meet or do not meet the criteria proposed in Refs. (10, 11).

In order to explain these artefacts we have suggested that the chemical reduction may coincide with activated H_2 adsorption–desorption phenomena. With respect to these adsorption–desorption processes, three hypotheses can be suggested: (i) hydrogen is adsorbed on the surface of metallic copper, (ii) hydrogen is either occluded inside the copper crystal lattice or retained by structural defects, and (iii) the hydrogen uptake is effected just by the copper oxides, especially by the partly reduced copper oxides.

Pritchard *et al.* (24) have reported that dissociative hydrogen chemisorption takes place on copper, high Miller index planes being more efficient in the H_2 dissociation than the (100), (111), and (110) low index planes. The last statement has been reconsidered by Pritchard on the basis of his more recent observations about a closer similarity between the (111) and the high-index faces (25). However, the activated nature of the hydrogen chemisorption on copper is by now clearly established, as shown by Balooch *et al.* (26), Greuter and Plummer (27), and recently by Winkler *et al.* (28). Activated hydrogen absorption on copper was recently observed also on both reduced Cu/Al_2O_3 and $Cu/ZnO/Al_2O_3$ catalysts by Muhler *et al.* (29) and on reduced Cu/ZnO catalysts by Roberts and Griffin (30). These latter authors showed that both reduced CuO and Cu/ZnO specimens have the most prominent H_2 desorption peak at 308–318 K, and calculated an apparent activation energy of desorption of 20 kcal mol^{-1} (30). Since the presumed desorption peak due to hydrogen evolution is positioned in the TPR profiles of CuO and Cu_2O in the temperature range 520–590 K (see shaded areas in Figs. 3A and 3D), all hydrogen should be desorbed at these relatively high temperatures.

Our second hypothesis is that even if hydrogen has completely desorbed at the surface of metallic copper, it may be more firmly retained inside the copper crystal lattice by bonding or trapping processes. As general ground, it is well known that metals with face (*fcc*) and body (*bcc*) centered cubic crystal structures may have many types of structural defects such as grain boundaries, dislocations, micro-voids, which can act as trap sites (31). Hydrogen can also be trapped at the interface of ferrite with carbides or non-metallic inclusions (Al,Si,Fe-oxides, TiC, MnS) (32), the latter representing the most effective trap sites. This phenomenon has been studied in particular for iron and steel (33, 34) in order to obtain insights into hydrogen embrittlement which causes very serious losses in the industry. Choo and Lee (35–37), by means of TPD and permeation experiments with pure iron and carbon steel, calculated the trap activation energy of hydrogen evolution from various trap sites as ranging from 18 to 35 kJ mol^{-1}. In another work, performed by TPD, Hong and Lee related a peak at 695 K to hydrogen trapped at the interfaces of iron oxide inclusions (38); the corresponding trap activation energy was found to be 47.2 kJ mol^{-1}.

Copper samples containing dissolved hydrogen have been prepared by quenching from equilibrium at higher temperature (39). However, residual trapped hydrogen bubbles have been found after annealing up to 420 K (39). Moreover, electron microscopy investigations showed that the hydrogen bubbles formed preferentially at grain boundaries and dislocations.

The following interpretation can thus be suggested: during a TPR run, and from the very start of the reduction process, formation and growth of the first nuclei of copper occur. Since hydrogen continuously flows over the copper crystallites freshly formed from CuO and Cu_2O, hydrogen can be trapped by copper structural defects, and/or can be occluded inside the metal while, in parallel, the reduction of the unreduced oxide particles goes on. As the temperature, and therefore the reaction rate, increases, more copper and hydrogen bubbles are formed, while

sintering of the metal crystallites also occurs. At temperatures high enough to overcome either the trap activation energy or to escape from the bubbles, hydrogen can desorb giving rise, at high K values, to the double peak through the previously described behavior of the hydrogen detector. This explanation is indeed supported by a very recent paper dealing with the outgassing characteristics of copper (40). In this work it was shown by thermal desorption spectroscopy (TDS) that hydrogen occluded in pure copper exhibited an abrupt rise of the desorption peak at the temperature of about 573 K (40).

The shaded area of the reduction profile of the TPR run 8A (see Fig. 3D, curve a) is about 6% of the total area of the reduction peak, by which the amount of desorbed hydrogen corresponds to approximately 50 μmol. If it is taken into account that (i) a lot of hydrogen can be captured by each trap site, (ii) the amount of copper is increasing while the TPR run proceeds, and (iii) the reduced copper is expected to be highly defective, the amount of desorbed hydrogen previously indicated seems to be fairly reasonable.

The third hypothesis is that the copper oxides, and especially the partly reduced copper oxides, are able to pick up relatively large quantities of hydrogen. Roberts and Griffin have given some evidence that both CuO and CuO/ZnO catalysts adsorb strongly hydrogen in the oxidized and partly reduced state (30). In their TPD spectra on reoxidized CuO and CuO/ZnO catalysts, H_2 desorption peaks appeared at relatively high temperatures (387–403 K), while for the reduced sample the H_2 desorption peaks were found at 308–318 K (30).

Our hypotheses concerning the role played by H_2 adsorption–desorption processes on the appearance of the artefacts are indirectly confirmed by the sequence of TPR profiles of CuO reported in Fig. 3D. It clearly appears that the shape of the TPR profiles is markedly modified on varying the heating rate. On going from higher to lower heating rates, the TPR profile, firstly characterized by a large and double peak shaped band, is progressively transformed into a single and Gaussian-type reduction peak, despite the high value of K. This result can be rationalized as follows. On decreasing the heating rate, the reduction rate at the peak maximum is drastically lowered as well as the value of the Malet and Caballero parameter P (11). Consequently, the fractional hydrogen conversion at the peak maximum decreases progressively to values well below the feed rate and, finally, at the lowest heating rate of 0.4 K min^{-1} becomes entirely consistent with the criteria for obtaining optimum reduction profiles (10). Of course, the concentration of H_2 at the reactor outlet increases on decreasing the heating rate, then the small amount of desorbed hydrogen will be diluted by the higher fraction of the unreacted hydrogen.

With respect to CuO–ZnO samples, the presence of zinc oxide may play a double role: on the one hand, sintering of the copper crystallites is prevented, affecting the amount of either trapped or precipitated hydrogen; on the other hand, the boundary layers of both Cu°–ZnO and Cu°–CuO–ZnO could manifest an influence on the hydrogen activation (23). A combination of these effects could prevent the evolution of H_2 in the stream so that a pronounced minimum is no longer formed and a broadening of the TPR peak prevalently occurs.

For completeness of the work one should note that situations may occur inside the pores in which, for large amounts of reducible species and for high fractional conversion of hydrogen, the considerable quantity of water abruptly released at the peak maximum can exceed its equilibrium content ($MeO + H_2 \leftrightarrow Me + H_2O$) blocking the reduction processes until more propitious conditions are reestablished with water desorption.

Regardless of the interpretation, the present experiments have provided evidence that adsorption–desorption phenomena, either of hydrogen or of water, can interfere with the real TPR peak profiles, so that the simple kinetic model (10, 11) of non-isothermal reduction needs an adsorption–desorption step for hydrogen in parallel with chemical reaction. The same approach and analysis can be applied to any reducible oxide used as catalyst, to provide correct interpretation of metal chemical states.

V. CONCLUSIONS

- Direct experimental evidence shows that TPR profiles are markedly perturbed by an inadequate combination of the initial amount of reducible species, total flow rate, initial hydrogen concentration, heating rate, and activation energy of the reaction.
- Under correct experimental conditions the reduction profiles of pure CuO and Cu_2O are characterized by single reduction peaks, which also represent the TPR pattern of CuO–ZnO catalysts in the range of atomic ratios Cu : Zn = 92 : 8 to 67 : 33. Contrary to this, when TPR measurements are carried out with values of the experimental operating variables improperly selected, artefacts, such as an apparent double-peak for CuO and Cu_2O and a profile broadening for the CuO–ZnO catalysts, disturb the reduction profiles so that the reliability of the results is completely lost.
- Broadening of TPR profiles takes place, as expected, when the ratio between the initial amount of reducible species and the feed rate of the reactor is very high. In this case the hydrogen consumption at the maximum reduction rate is very large and can result in the exhaustion of the hydrogen in the feed.
- Owing to both the dynamical situation, caused by the large fractional H_2 consumption, and to the H_2 (or H_2O)

adsorption–desorption phenomena, an unexpected double-peak appears in the reduction profiles of CuO and Cu_2O, which cannot be interpreted by a simple kinetic model. It is suggested that desorption of hydrogen, either trapped by structural defects, or precipitated in massive copper, or retained by the partly reduced copper oxides, could be responsible for the apparent double peak.

• A kinetic analysis of non-isothermal reductions was developed taking into account both the TPR dynamics and the hydrogen adsorption–desorption phenomena coinciding with the reduction process. Simple kinetic considerations derived from this analysis allowed us to reproduce qualitatively the shape of some perturbed TPR experimental profiles.

• Results of studies using the TPR technique need more critical attention than is often given to them.

REFERENCES

1. Robertson, S. D., McNicol, B. D., De Baas, J. H., Kloet, S. C., and Jenkins, J. W., *J. Catal.* **37,** 424 (1975).
2. Kadkhodayan, A., and Brenner, A., *J. Catal.* **117,** 311 (1989).
3. Delk II, F. S., and Vávere, A., *J. Catal.* **85,** 380 (1984).
4. Wagstaff, N., and Prins, R., *J. Catal.* **59,** 434 (1979).
5. Isaacs, B. H., and Petersen, E. E., *J. Catal.* **77,** 43 (1982).
6. Gentry, S. J., Hurst, N. W., and Jones, A., *J. Chem. Soc., Faraday Trans. 1* **77,** 603 (1981).
7. Brown, R., Cooper, M. E., and Whan, D. A., *Appl. Catal.* **3,** 177 (1982).
8. Sexton, B. A., Hughes, A. E., and Turney, T. W., *J. Catal.* **97,** 390 (1986).
9. Jones, A., and McNicol, B. D., *in* "Temperature-Programmed Reduction for Solid Materials Characterization," Dekker, New York, 1986.
10. Monti, D. A. M., and Baiker, A., *J. Catal.* **83,** 323 (1983).
11. Malet, P., and Caballero, A., *J. Chem. Soc., Faraday Trans. 1* **84,** 2369 (1988).
12. Fierro, G., Lo Jacono, M., Inversi, M., Porta, P., and Lavecchia, R., *in* "Proceedings, 10th International Congress on Catalysis, Budapest, 1992" (L. Guczi, F. Solymosi, and P. Tétényi, Eds.), p. 1847. Akadémiai Kiadó, Budapest, 1993.
13. Porta, P., De Rossi, S., Ferraris, G., Lo Jacono, M., Minelli, G., and Moretti, G., *J. Catal.* **109,** 367 (1988).
14. Porta, P., Fierro, G., Lo Jacono, M., and Moretti, G., *Catal. Today* **2,** 675 (1988).
15. Porta, P., Dragone, R., Lo Jacono, M., Minelli, G., and Moretti, G., *Solid State Ionics* **32/33,** 1019 (1989).
16. Klug, H. P., and Alexander, L. E., *in* "X-ray Diffraction Procedures for Polycrystalline and Amorphous Materials," Wiley, New York, 1954.
17. Herman, R. G., Klier, K., Simmons, G. W., Finn, B. P., Bulko, J. B., and Kobylinski, T. P., *J. Catal.* **56,** 407 (1979).
18. Ferraris, G., and De Rossi, S., *Appl. Catal.* **71,** 333 (1991).
19. Lo Jacono, M., Cimino, A., and Inversi, M., *J. Catal.* **76,** 320 (1982).
20. Cvetanović, R. J., and Amenomiya, Y., *in* "Advances in Catalysis" (D. D. Eley, H. Pines, and P. B. Weisz, Eds.), Vol. 17, p. 103. Academic Press, New York, 1967.
21. Ibok, E. E., and Ollis, D. F., *J. Catal.* **66,** 391 (1980).
22. Fleisch, T. H., and Mieville, R. L., *J. Catal.* **90,** 165 (1984).
23. Fierro, G., Lo Jacono, M., Inversi, M., Porta, P., Lavecchia, R., and Cioci, F., in preparation.
24. Pritchard, J., Catterick, T., and Gupta, R. K., *Surf. Sci.* **53,** 1 (1975).
25. Pritchard, J., *J. Chem. Soc., Faraday Trans. 1* **83,** 2249 (1987).
26. Balooch, M., Cardillo, M. J., Miller, D. R., and Stickney, R. E., *Surf. Sci.* **46,** 358 (1974).
27. Greuter, F., and Plummer, E. W., *Solid State Commun.* **48,** 37 (1983).
28. (a) Anger, G., Winkler, A., Rendulic, K. D., *Surf. Sci.* **220,** 1 (1989); (b) Rendulic, K. D., and Winkler, A., *Int. J. Mod. Phys. B* **3,** 941 (1989).
29. Muhler, M., Nielsen, P. L., Tornqvist, E., Clausen, B. S., and Topsøe, H., *Catal. Lett.* **14,** 241 (1992).
30. Roberts, D. L., and Griffin, G. L., *J. Catal.* **110,** 117 (1988).
31. Lee, J. Y., and Lee, J. M., *Surf. Coat. Technol.* **28,** 301 (1986).
32. Pressouyre, G. M., *Metall. Trans., A* **10,** 1571 (1979).
33. Kumnick, A. J., and Johnson, H. H., *Acta Metall.* **28,** 33 (1980).
34. Hirth, P. J., *Metall. Trans., A* **11,** 861 (1980).
35. Choo, W. Y., and Lee, J. Y., *J. Mater. Sci.* **17,** 1930 (1982).
36. Choo, W. Y., and Lee, J. Y., *Metall. Trans., A* **13,** 135 (1982).
37. Choo, W. Y., and Lee, J. Y., *Metall. Trans., A* **14,** 1299 (1983).
38. Hong, G. W., and Lee, J. Y., *Mater. Sci. Eng.* **61,** 219 (1983).
39. Wampler, W. R., Shober, T., and Lengeler, B., *Philos. Mag.* **34,** 129 (1976).
40. Kurosaka, A., Nakao, O., Yoshikawa, T., and Ueki, M., *J. Vac. Sci. Technol., A* **10(6),** 3465 (1992).